Search for features in the cosmic-ray electron and positron spectrum measured by the Fermi Large Area Telescope

M. N. Mazziotta, F. Costanza, A. Cuoco, F. Gargano, F. Loparco, and S. Zimmer

Search for Features in the Cosmic-Ray Electron and Positron spectrum measured by the Fermi Large Area Telescope

M. N. Mazziotta,[1, *] F. Costanza,[1, 2] A. Cuoco,[3, 4] F. Gargano,[1] F. Loparco,[1, 5] and S. Zimmer[6]

[1]*Istituto Nazionale di Fisica Nucleare, Sezione di Bari,*
via Orabona 4, I-70126 Bari, Italy
[2]*CNRS - Laboratoire d'Annecy de Physique des Particules,*
9 Chemin de Bellevue, F-74940 Annecy, France
[3]*RWTH Aachen University,*
Institute for Theoretical Particle Physics and Cosmology (TTK),
D-52056 Aachen, Germany
[4]*Istituto Nazionale di Fisica Nucleare, Sezione di Torino,*
via Pietro Giuria 1, I-10125 Torino, Italy
[5]*Dipartimento di Fisica "M. Merlin" dell'Università e del Politecnico di Bari,*
via Amendola 173, I-70126 Bari, Italy
[6]*University of Geneva,*
Département de physique nucléaire et corpusculaire (DPNC),
24 quai Ernest-Ansermet,
CH-1211 Genève 4, Switzerland

The Large Area Telescope onboard the Fermi Gamma-ray Space Telescope has collected the largest ever sample of high-energy cosmic-ray electron and positron events. Possible features in their energy spectrum could be a signature of the presence of nearby astrophysical sources, or of more exotic sources, such as annihilation or decay of dark matter (DM) particles in the Galaxy. In this paper for the first time we search for a delta-like line feature in the cosmic-ray electron and positron spectrum. We also search for a possible feature originating from DM particles annihilating into electron-positron pairs. Both searches yield negative results, but we are able to set constraints on the line intensity and on the velocity-averaged DM annihilation cross section. Our limits extend up to DM masses of 1.7 TeV/c^2, and exclude the thermal value of the annihilation cross-section for DM lighter than 150 GeV/c^2.

I. INTRODUCTION

During their propagation in our Galaxy, high-energy cosmic-ray electrons and positrons (CREs) lose their energy mainly through synchrotron radiation and inverse Compton interactions with the low-energy photons of the interstellar radiation field. Therefore, CREs reaching the Earth with energies above 100 GeV should be produced by a few nearby sources [1, 2]. Searching for anisotropies in the CRE spectrum provides a powerful probe for local sources, but current limits strongly disfavor the presence of local young and middle-aged astrophysical sources since such sources would produce large anisotropies [2].

An alternative production mechanism for high-energy CREs could arise due to the annihilation or decay of dark matter (DM), which would yield anisotropies in the CRE flux, albeit below the sensitivity of current analyses [3]. In this case, the CRE energy spectrum is expected to exhibit a cut-off at the energy corresponding to the DM mass [4]. This feature will still be visible in the spectrum after propagation. Therefore, the signature of a DM contribution to the CRE spectrum would be an "edge"-like feature at energies close to the DM mass.

Further features in the spectrum are expected from the fact that only a few astrophysical sources will contribute at the highest energies. In fact, CRE spectra of pulsars or supernova remnants are expected to be power laws with cut-offs, which vary from source to source. Thus the superposition of different sources will produce a final spectrum with bumps and dips, which will be more pronounced the fewer sources contribute [5]. The cut-offs are expected to be softer for these sources, with respect to the DM case, although, in practice, in the presence of a weak signal, it would be difficult to distinguish the two.

The CRE energy spectrum has been measured by several experiments, like AMS-02 [6], CALET [7], DAMPE [8] and the Fermi Large Area Telescope (LAT) [9–11]. Recently, the results of new measurements have been published, providing a confirmation of a break in the TeV region as previously seen by ground-based Cherenkov gamma-ray telescopes [12, 13] and an indication of a potential feature at 1.4 TeV (DAMPE).

The CRE data from the Large Area Telescope (LAT) onboard the Fermi satellite [14–16] have already been used to measure the energy spectrum [9–11], to search for anisotropies [1, 2] and for a possible excess from the Sun [17]. In this paper we have analyzed the same data sample used in the measurement of the CRE energy spectrum reported in Ref. [11] for the high-energy

analysis (standard path-length selection).[1]

In this analysis for the first time we use the Fermi-LAT CRE data to search for possible features in the spectrum originating from the direct annihilation of DM particles into e^+e^- pairs. In particular, as will be illustrated in Sec. III, we will search for either delta-like lines or for spectral edges. In the past, several attempts [18–20] were made to constrain scenarios with DM particles annihilating or decaying to leptonic final states using the measurements of CRE spectra performed by various experiments. In particular, in Refs. [21, 22] the CR positron ratio and the separate positron and electron fluxes measured by the AMS-02 experiment were used to constrain direct DM annihilations into e^+e^-. The LAT CRE data extend to higher energies than those from AMS-02, thus allowing us to set constraints for higher DM masses.

II. SPECTRUM OF COSMIC-RAY ELECTRONS AND POSITRONS FROM DM ANNIHILATIONS

To evaluate the spectrum of CREs produced from DM annihilations in the Galaxy, we used a customized version of the propagation code DRAGON [23–25], in which the cross sections for the production of secondary particles are taken from Ref. [26]. We set the propagation model of CRs in the Galaxy assuming the source term distribution from Ref. [27], while the gas density distribution and the interstellar radiation field (ISRF) are taken from the public GALPROP version [28–30]. The Galactic magnetic field model (GMF) is taken from Ref. [31].

We adopted a 3D version of the DRAGON code including a spiral arms model [32] that superimposes the spatial pattern of the distribution of different astrophysical quantities (e.g. source term, gas, ISRF and magnetic field) [33]. In our simulation we assume that the interstellar medium is composed of Hydrogen and Helium with relative abundances 1 : 0.1.

We assume that the scalar diffusion coefficient depends on the particle rigidity R and on the distance from the Galactic plane z according to the parametrization $D = D_0 \beta^\eta (R/R_0)^\alpha e^{|z|/z_t}$ [38]. We set $\alpha = 0.33$ according to the recent boron to carbon ratio (B/C) from the AMS-02 data [37], $R_0 = 4$ GV and $z_t = 4$ kpc, while D_0 and η are tuned to the B/C AMS-02 data, also setting the nuclei injection spectra to reproduce the VOYAGER 1 data at low energy [34, 35]. We have found that the B/C data are reproduced setting $D_0 = 7.4 \times 10^{28}$ cm² s⁻¹ and $\eta = -0.1$. A reacceleration model is also adopted to reproduce the B/C data at low energy, setting the Alfvén velocity to $v_A = 52$ km s⁻¹. The solar modulation is treated using the force-field approximation [39] with
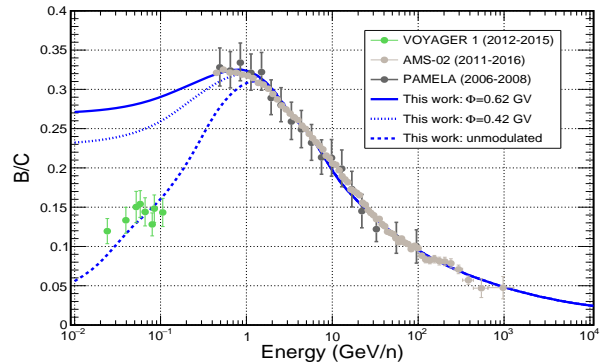

FIG. 1. Comparison of the predictions from the propagation model with boron to carbon ratio (B/C) data observed near the Earth. Dashed line: unmodulated intensity; dotted (solid) line: modulated intensity by means of the force field approximation with $\Phi = 0.42$ (0.62) GV, respectively. The plots show the data from VOYAGER 1 [34, 35], PAMELA [36] and AMS-02 [37].

$\Phi = 0.42$ GV and $\Phi = 0.62$ GV to reproduce the PAMELA and AMS-02 data respectively, which were taken at different parts of the solar cycle.

Figure 1 shows the comparison of the predictions from the actual propagation model with B/C data observed near the Earth by PAMELA [36] and by AMS-02 [37], and outside the solar system by VOYAGER 1 [34, 35] (unmodulated model).

We have used our model to propagate the CREs produced by DM annihilations in our Galaxy using the DRAGON code. We assume a Navarro–Frenk–White (NFW) DM density profile [40] with a local DM density $\rho_\odot = 0.41$ GeV cm⁻³ [41], and an annihilation cross section $\langle\sigma v\rangle = 3 \times 10^{-26}$ cm³ s⁻¹. The inclusive yields of $e^\pm$ from DM annihilations are taken from [4], including electroweak corrections [42]. Fig. 2 shows, for each DM mass, the expected CRE spectra at Earth (scaled by a factor of 10, i.e. they correspond to $\langle\sigma v\rangle = 3 \times 10^{-25}$ cm³ s⁻¹) compared with the Fermi LAT [11], AMS02 [6], CALET [7] and DAMPE [8] data. The DM spectra have been modulated using the force-field approximation with a modulation potential $\Phi = 0.55$ GV. This value has been derived based on an analysis of gamma rays coming from the Moon using the same time range as considered in this paper [43]. The DM spectra are used as templates in the fit procedure described in Sec. III. For different $\rho_\odot$, constraints will rescale as $\rho_\odot^2$.

We have also used the 2D version of DRAGON [33] in which the diffuse equation is solved in cylindrical coordinates with azimuthal symmetry and without spiral arms. In this way we can check for the effects of uncertainties related to propagation on the DM spectra. We used the same values of R_0, z_t as in the 3D model, while the remaining parameters have been adjusted to

---

[1] The data set has been collected between August 4, 2008, and June 24, 2015. The full details of the event selection are reported in Ref. [11].
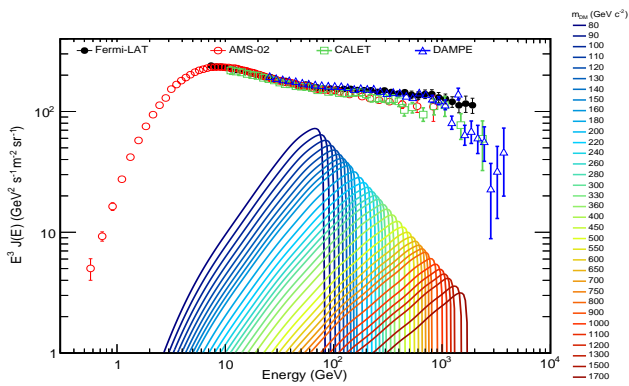
FIG. 2. CRE spectra at Earth. The expected contributions from possible DM annihilations in the Galaxy (see text) are compared with the data from the Fermi LAT [11], AMS-02 [6], CALET [7] and DAMPE [8].

the B/C data. In particular we found $\alpha = 0.42$, resulting in DM spectra lower by about 20% or less with respect to those evaluated with the 3D model of the Galaxy. We have tested also 2D models with different z_t from 2 kpc to 7 kpc. In this case the effect is smaller, at the level of 10%.

Further uncertainties come from the ISRF and the GMF. We have studied them changing separately the normalization of the ISRF and magnetic field by $\pm50\%$, which resulted in a $[-50\%, +100\%]$ variation in the normalization of DM spectra. A similar study has been performed in Ref. [21] yielding comparable results.

We have also tested for a different DM profile, namely an isothermal profile, still normalized to the same local DM density. Differences in this case are even smaller (few percent).

III. ANALYSIS METHOD

Following the approach of Ref. [44], we have implemented a fitting procedure in sliding energy windows to search for possible local peaks (either bumps or lines) on top of a smooth CRE spectrum.

In each energy window we model the CRE intensity as $I(E) = I_0(E) + I_f(E)$, where $I_0(E)$ is the "smooth" part of the spectrum and $I_f(E)$ describes the possible feature. Since the energy windows are narrow, we assume that the smooth part of the spectrum can be described by a power-law (PL) model $I_0(E) = k(E/E_0)^{-\gamma}$, where γ is the PL spectral index and the prefactor k corresponds the CRE intensity at the scale energy E_0, fixed to 1 GeV.

In our analysis, we assume two models for $I_f(E)$: (i) a delta-like (line) model $I_f(E) = s\delta(E - E_{line})$, where s represents the line intensity; (ii) a spectrum produced by DM annihilating into CREs $I_f(E) = sI_{DM}(E|m_{DM}, \langle\sigma v\rangle, ...)$, where $I_{DM}(E)$ is the intensity of CREs from DM observed near the Earth, which is

calculated in Sec. II, and the parameter s represents the scale of the annihilation cross-section implemented in the model. In this case s corresponds to $\langle\sigma v\rangle$ in units of 3×10^{-26} cm^3 s^{-1}. The line model is used as a generic model for a feature. It can represent DM spectra from alternative DM models, or also features induced by local nearby astrophysical sources.

Starting from the model, we can calculate the expected counts in each CRE observed energy bin E_j as:

$$\mu_j = \mu(E_j) = t \int dE\ \mathcal{R}(E_j|E)\ I(E) \qquad (1)$$

where E is true (Monte Carlo) energy, $\mathcal{R}(E_j|E)$ is the instrument response matrix (acceptance) which incorporates the energy resolution of the LAT, and t is the integrated livetime.

For our fitting procedure we define a χ^2 function as follows:

$$\chi^2 = \sum_{j=1}^{N} \frac{(n_j - \mu_j)^2}{n_j + f_{syst}^2 n_j^2} \qquad (2)$$

where N is the number of energy bins used for the fit. The denominator of each term in the summation includes the sum in quadrature of the statistical Poisson fluctuations ($\sqrt{n_j}$) and systematic uncertainties ($f_{syst}n_j$), which are discussed more in detail below.

To estimate the parameters $\{k, \gamma, s\}$ which minimize the χ^2 we use the MINUIT code within the ROOT toolkit [45, 46]; the values of the parameters at a 95% confidence limit (CL) are evaluated using MINOS and setting the error confidence level to 2.71.

We have scanned an energy range extending from 42 GeV to 2 TeV.[2] This interval has been divided in 64 bins per decade, equally spaced on a logarithmic scale. When searching for line features, we selected fit windows centered on the line energy E_{line} with a half-width of $0.35E_{line}$. Once folded with the energy response, a delta-like line will show up as a broad peak in the count spectrum with the same width as the energy resolution of the LAT, which is always less than the window size[3]. On the other hand, when searching for a DM signal, we selected fit windows centered on the candidate DM mass m_{DM} with a half-width of $0.5m_{DM}$. Since a feature originating from DM (Sec. II) will be spread across a larger energy interval than a line, we chose a larger fit window than in the line search. We also tested different energy binnings and different window

---

[2] The limits of 42 GeV and 2 TeV are the same as in the high-energy event selection in Ref. [11].

[3] The LAT energy resolution for the CRE selection at 95% containment ranges from about 15% at 42 GeV to about 20% at 1 TeV and increases up to 35% at 2 TeV [11].
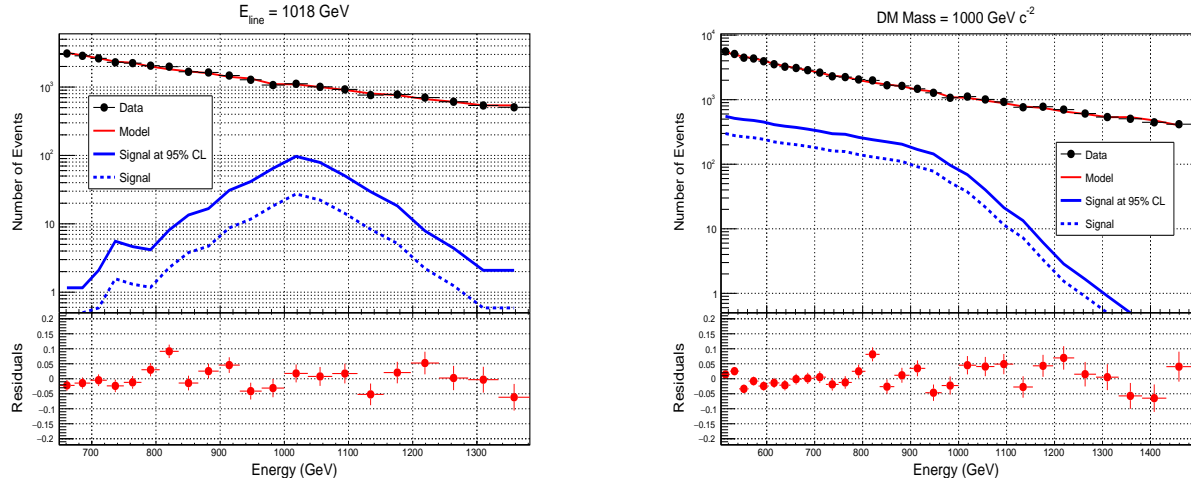
FIG. 3. Example of fit results near 1 TeV. The left plot is obtained fitting the CRE spectrum with a delta-like line feature on top of a PL spectrum; the right plot is obtained assuming a feature due to DM annihilating into CREs on top of a PL spectrum. The top panels of each plot show a comparison of the measured counts (black points) with those predicted from the fit (red solid line). The contributions from the possible features are also shown: the blue dashed lines indicate the counts originated from the feature when the best fit value for the parameter s is assumed; the blue solid lines indicate the counts originated from the feature when the upper limit at 95% confidence level for s is assumed. The bottom panels show the fit residuals as a function of energy. The error bars include only the statistical uncertainties.

sizes yielding comparable results. The details of these studies are given in Appendix A.

The high-energy CRE sample used in the present analysis is affected by systematic uncertainties. In Ref. [11] it was shown that the fractional systematic uncertainty f_{syst}, due to the acceptance calculation, to the proton contamination and to the data/Monte Carlo corrections (added in quadrature) ranges from about 1.3% at 42 GeV to about 15% at 2 TeV. In Ref. [11] the calculation of f_{syst} was performed dividing the energy interval in 16 bins per decade and the statistical uncertainties were always found to be about one of order of magnitude less than systematic ones.

To account for systematic uncertainties, that might mimic a false local feature signal or might mask a true local feature, we have implemented a data-driven procedure.[4] As a starting point we have fitted the data, in a given window, with a PL model considering statistical uncertainties only. Then we have evaluated the fractional residuals $f_j = (n_j - \mu_j)/\mu_j$, where n_j is the number of CRE events in the j-th observed energy bin (E_j) and μ_j is the number of CRE events predicted by the PL model. We have then built the distribution of fractional residuals and we have calculated its root mean square (RMS). Finally, we have derived the systematic uncertainties f_{syst} from the difference between the observed RMS and its expected

value when only statistical uncertainties are considered.[5] We note that this is expected to slightly reduce the sensitivity to a possible spectral feature, since the feature would contribute to the evaluation of the systematic uncertainties. In the case of a non-detection, this would result in conservative limits.

For each energy window we evaluate the significance of a possible feature considering the χ^2 difference between the alternative hypothesis (line or DM signal) and the null hypothesis (PL model) as Test Statistics. In addition we evaluate the expectation bands for our results, i.e. the sensitivity to the null hypothesis, using a pseudo-experiment technique. As a starting point, we fit the observed CRE count distribution with a simple PL model in the whole energy range.[6] This model is used as a template to evaluate the expected counts in each energy bin. Starting from the template model, a set of 1000 pseudo-experiments is performed, in which the counts in each energy bin are extracted from a Poisson distribution with mean value taken from the template, after adding a gaussian fluctuation to account for energy-dependent systematic uncertainties. The count distributions corresponding to the various pseudo-experiments are then fitted including the feature, and the containment bands (quantiles) for all the parameters are calculated.

————

[4] Since no control measurements are available, we cannot evaluate systematic uncertainties following an approach like the one used in Ref. [44].

————

[5] The RMS on the distribution of fractional residuals can be expressed as $f_{RMS}^2 = f_{stat}^2 + f_{syst}^2$.

[6] As shown in Ref. [11], the CRE energy spectrum above 50 GeV is well described by a single power law.
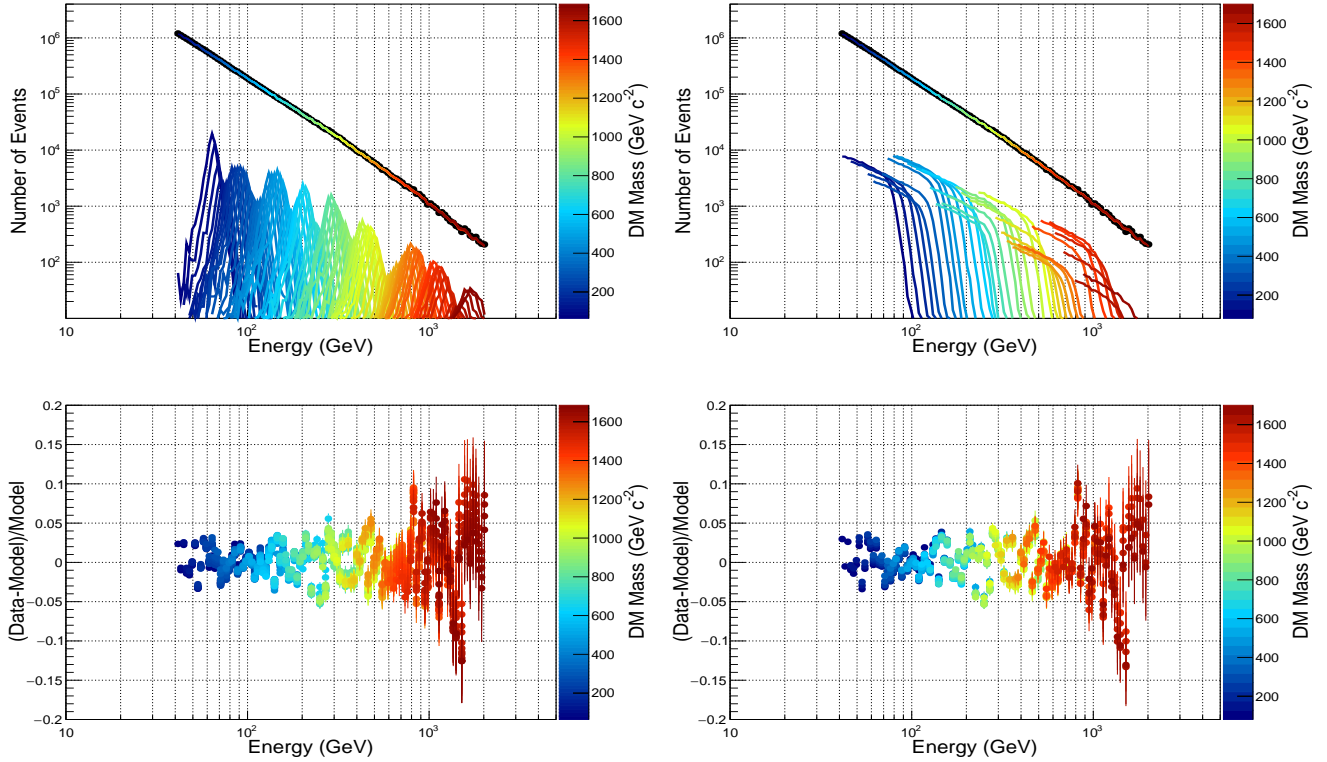
FIG. 4. Comparison of the fitted CRE spectra with the data. The left plots have been obtained fitting the CRE spectrum with a delta-like line feature on top of a PL spectrum; the right plots have been obtained assuming a feature due to DM annihilating into CREs on top of a PL spectrum. Different colors correspond to different values of E_{line} or m_{DM} and, consequently, to different energy windows. The top plots show a comparison of the measured count spectra (black points) with the fitted ones (colored bands). The contributions from the features at 95% CL limit are also shown in the plots as continuous solid lines. The bottom plots show the count residuals in the various energy windows. The error bars include only the statistical uncertainties.

IV. RESULTS AND DISCUSSION

Fig. 3 shows the results of the fits performed in the energy region near 1 TeV. The left and right plots show respectively the results obtained when the CRE spectrum is fitted with a delta-like line feature or with a DM feature on top of a PL spectrum. The figures show a comparison of the measured counts with those predicted from the fit. In both cases the fitted count distributions reproduce fairly well the observed ones. In the figures the contributions to the count spectra from the features are also shown. The counts due to the possible feature are always less than the 10% of the total counts in each bin.

A comparison of the fitted spectra with the data is shown in Fig. 4. The plots in the left panels show the results obtained when fitting the CRE count distribution with a delta-like line feature on top of a PL spectrum, while those in the right panels show the results obtained when fitting the distribution with a feature due to DM annihilations in the Galaxy superimposed on a PL spectrum. In both cases, the observed count spectrum is well reconstructed in all the energy windows.

A summary of the fit results is given in Fig. 5. In the top and in the middle panels the values of the fitted PL prefactor (k) and spectral index (γ) are shown as a function of energy for the two spectral models considered in the present analysis. The left plots show the results obtained for the delta-like line feature, while those on the right show the results obtained assuming a feature in the CRE spectrum due to DM annihilating into CREs. The values of the parameters obtained in the fit are compared with those obtained when the fit is performed without the feature, setting $I_f(E) = 0$ or equivalently $s = 0$ (null hypothesis). The values of k and γ obtained in the null hypothesis are consistent with those obtained when $s \neq 0$. This result is expected, since possible spectral features are expected to be tiny. The plots in Fig. 5 also show the confidence belts evaluated with the pseudo-experiment technique described in Sec. III. In most cases the fitted parameters lie within the central 95% confidence belt.

As mentioned in Sec. III, to evaluate the local significance of a possible feature one can use as a Test Statistic the value $TS_{local} = -\Delta\chi^2 = -(\chi_1^2 - \chi_0^2)$ where χ_1^2 and χ_0^2 are respectively the χ^2 values obtained when fitting the data with the alternative hypothesis (line or
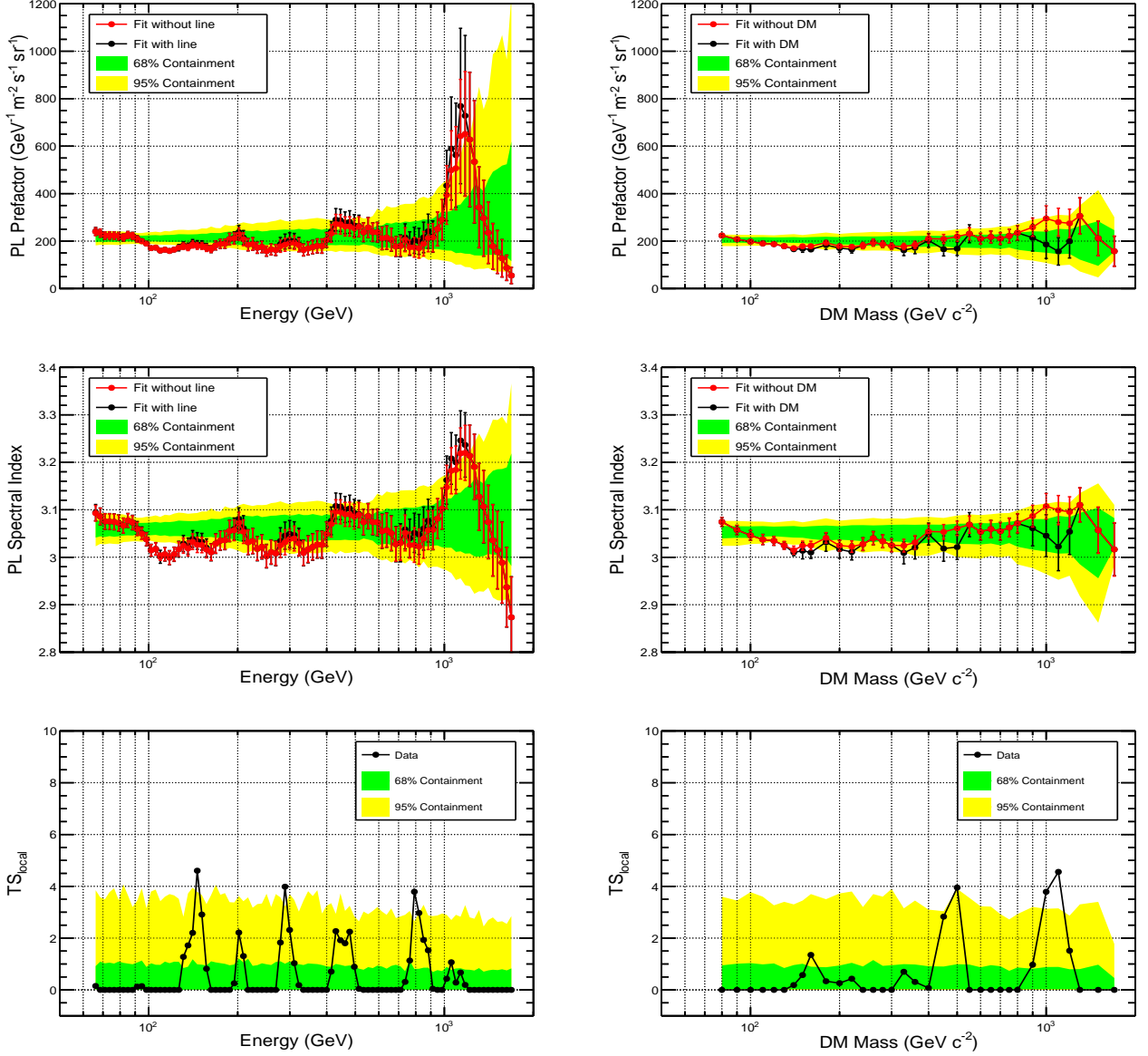
FIG. 5. Summary of the fit results. The left plots have been obtained fitting the CRE spectrum with a delta-like line feature on top of a PL spectrum; the right plots have been obtained assuming a feature due to DM annihilating into CREs on top of a PL spectrum. The black points in the top four plots indicate the values of the PL prefactor and spectral index obtained when the feature is included in the fit; the red points are obtained when the fit is performed without the feature, i.e. setting $I_f(E) = 0$. The bottom plots show the values of the Test Statistics $TS_{\rm local}$ for the line (left) and DM (right) models (alternative hypothesis) with respect to the simple PL model (null hypothesis). The green and yellow bands indicate the 68% and 95% confidence belts evaluated with the pseudo-experiment technique.

DM signal superimposed to the PL spectrum) and with the null hypothesis (PL spectrum). The $TS_{\rm local}$ defined in this way is expected to obey a χ^2 distribution with one degree of freedom since the two models differ by one free parameter. The local significance in σ units can be then evaluated as $s_{\rm local} = \sqrt{TS_{\rm local}}$.

The bottom panels of Fig. 5 show the values of $TS_{\rm local}$ as a function of energy, compared with the 68% and 95% expectation bands obtained with the pseudo-experiment technique. In most energy windows, the values of $TS_{\rm local}$

are close to zero and lie within the 95% expectation band. There are some fits yielding values of $TS_{\rm local}$ slightly above the 95% expectation bands. However, in the evaluation of the global significance of these possible features, it should be kept in mind that the fits are not independent and the number of trials should be taken into account. As a consequence, possible features associated with a local significance larger than 2σ turn out to be globally insignificant. The local significance of a possible feature has been evaluated from $TS_{\rm local}$.
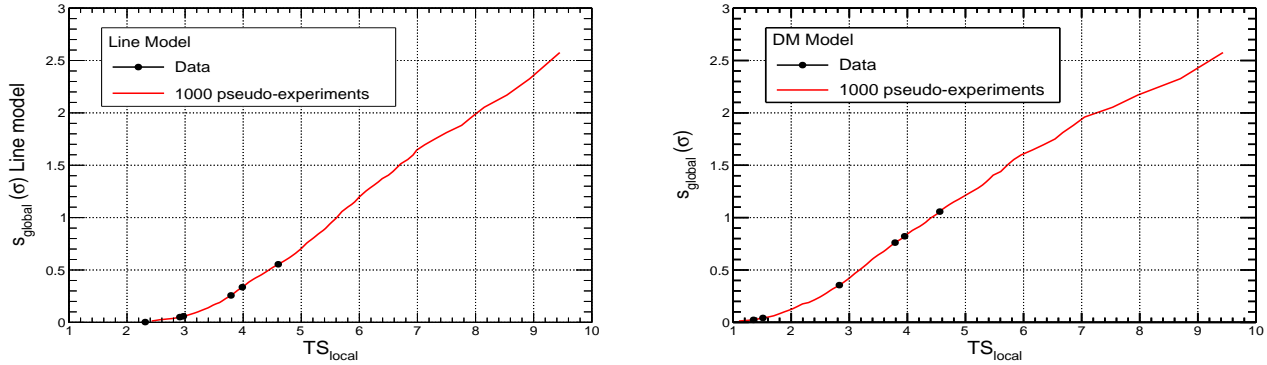
FIG. 6. Conversion from TS_{local} to s_{global} derived from the analysis of the 1000 pseudo-experiments. Left panel: line model. Right panel: DM model. The markers show some of most statistically significant local features.

However, since we perform many fits, to obtain the global significance s_{global}, the local significance must be corrected taking into account the effective number of trials. For the line search we performed 88 fits, while for the DM search we performed 32 fits, but all these fits are not independent since they largely overlap in energy.

To calculate the global significances we use the 1000 pseudo-experiments discussed in Sec. III. For each pseudo-experiment (which corresponds to a simulation of one full search across the entire energy range) we record the largest value of the local Test Statistic, TS_{max}. We then calculate the quantiles of the distribution of TS_{max} and we evaluate the corresponding values of the global significance s_{global} assuming that s_{global} obeys a a half-normal distribution.

Fig. 6 shows the conversion from TS_{local} to s_{global} for the line (left panel) and DM (right panel) models. The most significant features have global significances of 0.56σ ($E = 145$ GeV) and 1.14σ ($m_{DM} = 1.1$ TeV/c^2) for the line and DM model respectively.

Fig. 7 shows the upper limits at 95% confidence level on the parameters describing the feature (s for the line, $\langle \sigma v \rangle$ for the DM signal). In the right panel of Fig. 7 we also include dashed-dotted and dotted black lines showing variations of the limits on $\langle \sigma v \rangle$ assuming that $\rho_\odot$ can vary in the range $(0.25 - 0.7)$ GeV cm^{-3} and that the ISRF together with the GMF can vary by $\pm 50\%$, respectively. The green and yellow bands show the 68% and 95% CL expectation bands, respectively, calculated from the pseudo-experiments discussed in Sec. III. Since the limits lie within the 95% CL expectation bands, the Fermi LAT data do not provide evidence of any feature at the 2σ (local) level, either in the case of a delta-like line or in the case of a signal from DM annihilations in the Galaxy.

As shown in Fig. 2, the differences among the CRE spectra measured by DAMPE, CALET, AMS-02 and the Fermi LAT are within 20% in the TeV region. Assuming this uncertainty on the CRE spectrum, this would imply a variation of the current upper limits at most at the same

level, which is significantly smaller than the variations originating from the uncertainties in the DM models, due to for instance the uncertainties on the local DM density, or to those on the GMF and on the ISRF. Although our analysis of the LAT data accounts for systematic uncertainties, in the most conservative interpretation, it could be argued that the 20% differences represent the limit to what could be resolved.

The 95% upper limits on the velocity-averaged DM annihilation cross section $\langle \sigma v \rangle$ into $e^+ e^-$ pairs obtained in the present analysis lie below the thermal relic cross section calculated by Steigman et al. [47] for DM masses up to 100 GeV/c^2. Our limits are consistent with those obtained by Bergström et al. in Ref. [21] when studying the AMS-02 data on the positron fraction [51] and by Cavasonza et al. in Ref. [22] when studying the AMS-02 electron and positron data [52] in the range around 100 GeV where they overlap in energy.[7]

The present limits are also competitive with those obtained by the Fermi LAT Collaboration when studying the gamma-ray emission from the Virgo Galaxy Cluster [49] and from the Milky Way dwarf spheroidal Galaxies [48, 53] in the channel $e^+ e^- \gamma$ and are similar to those in the $b\bar{b}$ channel [48, 53]. Finally, our limits are consistent with the limits obtained from the analysis of the gamma rays from the inner Galactic halo performed by the H.E.S.S. Collaboration assuming a cuspy DM profile [50].

V. SUMMARY

In this work, we have used the Fermi-LAT CRE data to search for possible features in the spectrum originating from the direct annihilation of DM particles into $e^+ e^-$ pairs in the Galaxy halo. We searched for spectral

---

[7] In Refs. [21] and [22] the local DM density was assumed to be 0.4 GeV cm^{-3} and 0.3 GeV cm^{-3} respectively.
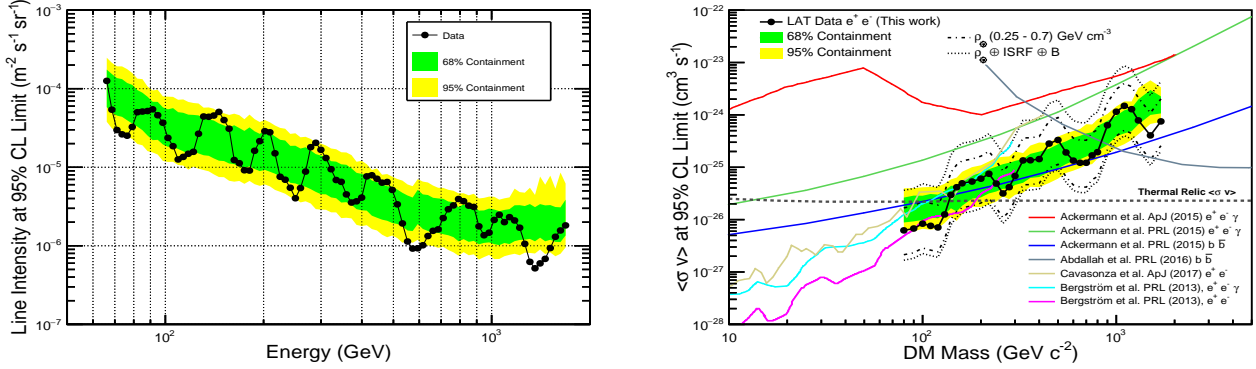
FIG. 7. Upper limits on the CRE spectral features. The left plot has been obtained assuming a delta-like line feature on top of a power-law spectrum; the right plot has been obtained assuming a feature due to DM annihilating into CREs on top of a power-law spectrum. The plots show the upper limits at 95% CL on the parameter describing the feature (s for the line, $\langle\sigma v\rangle$ for the DM signal). The dashed-dotted and the dotted black lines in the right plot indicate the variations of the limits on $\langle\sigma v\rangle$ for reasonable variations of the local DM density, of the ISRF and of the GMF (see discussion in the text). The green and yellow 68% and 95% confidence belts have been evaluated with the pseudo-experiment technique. The dashed line in the right plot indicates the thermal relic cross section from Steigman et al. [47]. The colored lines indicate the upper limits on $\langle\sigma v\rangle$ taken from Refs. [21, 22, 48–50].

features from 42 GeV to 2 TeV, thus extending the previous results based on the AMS-02 electron-positron data in the energy range above 300 GeV [21, 22]. The current results have been also compared with the constraints based on the DM annihilation to gamma rays.

The current analysis yields no evidence for a line or a DM feature. With the DM model assumed in the present analysis or for a pure line case, we do not find any indication for the presence of a feature at 1.4 TeV, as suggested by the recent DAMPE measurements [54–57].

The limits on the intensity of a line-like feature can be used, in principle, to study other DM models which also produce a feature in the spectrum. In this case, from an approximate match of the DM feature with the line, constraints on the DM model can be derived. Similarly, they can also be used to derive constraints on the presence of nearby CRE accelerators, like pulsars or supernova remnants. A quantitative analysis lies, however, beyond the scope of the present work.

Limits in the case of decaying DM with mass $2m$ can be easily obtained from the case of annihilating DM of mass m with the simple transformation: $\Gamma = 1/2\langle\sigma v\rangle\rho_\odot/m$, where Γ is the DM decay rate. We have explicitly checked that this approximation is valid at a few percent level or less.

Appendix A: Effects of the energy binning and of the window size on the constraints

To test the reliability of our analysis method, we have also studied the dependence of the fit results on the energy binning and on the choice of the window size. Fig. 8 shows a comparison of the upper limits on the line intensity and on the DM velocity averaged cross section $\langle\sigma v\rangle$ obtained dividing the energy interval in 32, 64 and 128 bins per decade and assuming the nominal sizes for the fit windows (i.e. $0.35E_{line}$ and $0.5m_{DM}$). As can be seen from the figure, in both cases the upper limits are almost independent of the energy binning.

In Fig. 9 we compare the upper limits on the line and on the DM annihilation cross sections obtained dividing the energy interval in 64 bins per decade and assuming
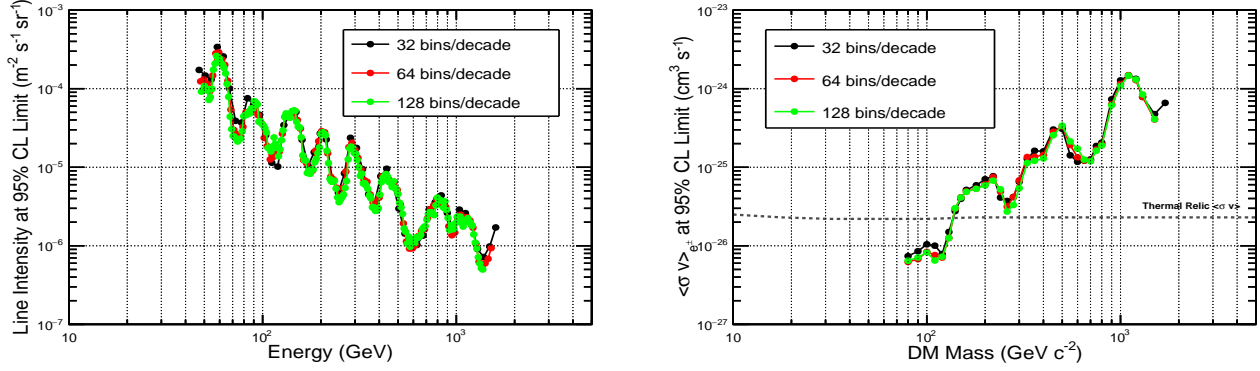
FIG. 8. Comparison of the upper limits at 95% confidence level on the line intensity (left plot) and on the velocity averaged cross section ⟨σv⟩ (right plots) obtained with 32 (black symbols), 64 (red symbols) and 128 (green symbols) energy bins per decade. The half-width of the fit windows is $0.35E_{line}$ for the line fits and $0.5m_{DM}$ for the DM fits.
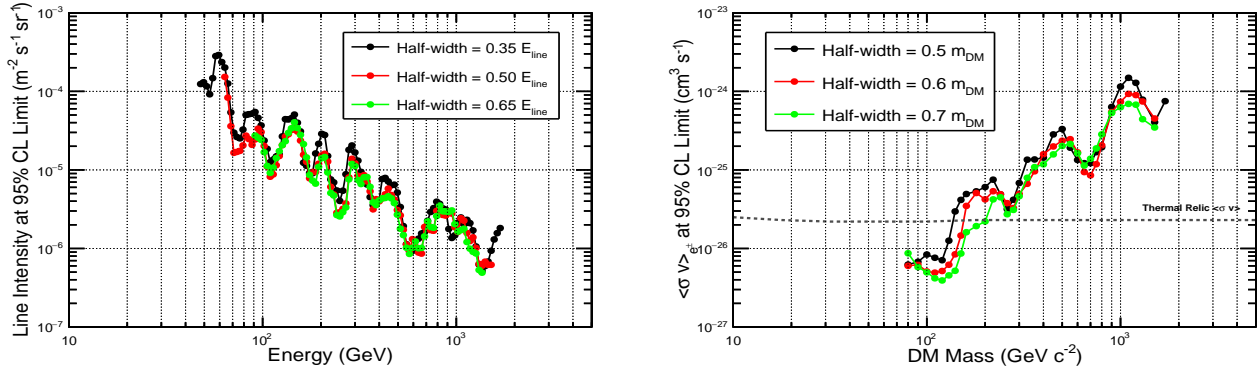

FIG. 9. Comparison of the upper limits at 95% confidence level on the line intensity (left plot) and on the velocity averaged cross section ⟨σv⟩ (right plots) obtained with fit windows of different widths. The fits have been performed dividing the whole energy interval in 64 bins per decade.

different sizes for the fit windows. In the case of the line fit, the upper limits are almost independent on the window size. The choice of the window size determines the interval $[E_{l1}, E_{l2}]$ of possible line energies, since the conditions $E_{l1} - \Delta E_{l1} \geq 42$ GeV and $E_{l2} + \Delta E_{l2} \leq 2$ TeV have to be satisfied, and larger window sizes will result in smaller energy intervals. Since the obtained line intensity is found to be independent of the chosen window size, we choose the smallest possible window size, $0.35E_{line}$.

Smaller windows are not appropriate for this analysis since, due to the energy resolution (15% − 35%), the line features are expected to spread over several energy bins, which should all be included in the fit windows. Likewise, for the DM fit, the obtained upper limits on the DM-induced flux show a mild dependence on the window size. In our analysis we choose a window size of $0.5m_{DM}$ since it provides the most conservative limits. Also in this case smaller windows are not appropriate because the feature is expected to spread over many energy bins.

[1] M. Ackermann et al. (Fermi-LAT Collaboration), Phys. Rev. D82, 092003 (2010), arXiv:1008.5119 [astro-ph.HE].
[2] S. Abdollahi et al. (Fermi-LAT), Phys. Rev. Lett. 118, 091103 (2017), arXiv:1703.01073 [astro-ph.HE].
[3] E. Borriello, L. Maccione, and A. Cuoco, Astropart. Phys. 35, 537 (2012), arXiv:1012.0041 [astro-ph.HE].
[4] M. Cirelli, G. Corcella, A. Hektor, G. Hutsi, M. Kadastik, P. Panci, M. Raidal, F. Sala, and A. Strumia, JCAP

1103, 051 (2011), [Erratum: JCAP1210,E01(2012)], arXiv:1012.4515 [hep-ph].
[5] D. Grasso et al. (Fermi-LAT Collaboration), Astropart. Phys. 32, 140 (2009), arXiv:0905.0636 [astro-ph.HE].
[6] M. Aguilar et al. (AMS), Phys. Rev. Lett. 113, 221102 (2014).
[7] O. Adriani et al. (CALET), Phys. Rev. Lett. 119, 181101 (2017), arXiv:1712.01711 [astro-ph.HE].
[8] G. Ambrosi et al. (DAMPE), Nature 552, 63 (2017),

arXiv:1711.10981 [astro-ph.HE].

[9] A. A. Abdo *et al.* (Fermi-LAT), Phys. Rev. Lett. **102**, 181101 (2009), arXiv:0905.0025 [astro-ph.HE].

[10] M. Ackermann *et al.* (Fermi-LAT Collaboration), Phys. Rev. Lett. **108**, 011103 (2012), arXiv:1109.0521 [astro-ph.HE].

[11] S. Abdollahi *et al.* (Fermi-LAT), Phys. Rev. **D95**, 082007 (2017), arXiv:1704.07195 [astro-ph.HE].

[12] F. Aharonian *et al.* (H.E.S.S.), Phys. Rev. Lett. **101**, 261104 (2008), arXiv:0811.3894 [astro-ph].

[13] F. Aharonian *et al.* (H.E.S.S.), Astron. Astrophys. **508**, 561 (2009), arXiv:0905.0105 [astro-ph.HE].

[14] W. B. Atwood *et al.* (Fermi-LAT Collaboration), Astrophys. J. **697**, 1071 (2009), arXiv:0902.1089 [astro-ph.IM].

[15] A. A. Abdo *et al.* (Fermi-LAT), Astropart. Phys. **32**, 193 (2009), arXiv:0904.2226 [astro-ph.IM].

[16] M. Ackermann *et al.* (Fermi-LAT), Astrophys. J. Suppl. **203**, 4 (2012), arXiv:1206.1896 [astro-ph.IM].

[17] M. Ajello *et al.* (The Fermi LAT), Phys. Rev. **D84**, 032007 (2011), arXiv:1107.4272 [astro-ph.HE].

[18] M. Di Mauro, F. Donato, N. Fornengo, and A. Vittino, JCAP **1605**, 031 (2016), arXiv:1507.07001 [astro-ph.HE].

[19] L. Bergstrom, J. Edsjo, and G. Zaharijas, Phys. Rev. Lett. **103**, 031103 (2009), arXiv:0905.0333 [astro-ph.HE].

[20] L. Feng, Q. Yuan, X. Li, and Y.-Z. Fan, Phys. Lett. **B720**, 1 (2013), arXiv:1206.4758 [astro-ph.HE].

[21] L. Bergstrom, T. Bringmann, I. Cholis, D. Hooper, and C. Weniger, Phys. Rev. Lett. **111**, 171101 (2013), arXiv:1306.3983 [astro-ph.HE].

[22] L. A. Cavasonza, H. Gast, M. Kramer, M. Pellen, and S. Schael, Astrophys. J. **839**, 36 (2017), arXiv:1612.06634 [hep-ph].

[23] C. Evoli, D. Gaggero, D. Grasso, and L. Maccione, JCAP **0810**, 018 (2008), [Erratum: JCAP1604,no.04,E01(2016)], arXiv:0807.4730 [astro-ph].

[24] D. Gaggero, L. Maccione, G. Di Bernardo, C. Evoli, and D. Grasso, Phys. Rev. Lett. **111**, 021102 (2013), arXiv:1304.6718 [astro-ph.HE].

[25] https://github.com/cosmicrays.

[26] M. N. Mazziotta, F. Cerutti, A. Ferrari, D. Gaggero, F. Loparco, and P. R. Sala, Astropart. Phys. **81**, 21 (2016), arXiv:1510.04623 [astro-ph.HE].

[27] K. M. Ferriere, Rev. Mod. Phys. **73**, 1031 (2001), arXiv:astro-ph/0106359 [astro-ph].

[28] A. W. Strong and I. V. Moskalenko, Astrophys. J. **509**, 212 (1998), arXiv:astro-ph/9807150 [astro-ph].

[29] I. V. Moskalenko, A. W. Strong, J. F. Ormes, and M. S. Potgieter, Astrophys. J. **565**, 280 (2002), arXiv:astro-ph/0106567 [astro-ph].

[30] http://galprop.stanford.edu/.

[31] M. S. Pshirkov, P. G. Tinyakov, P. P. Kronberg, and K. J. Newton-McGee, Astrophys. J. **738**, 192 (2011), arXiv:1103.0814 [astro-ph.GA].

[32] T. Y. Steiman-Cameron, M. Wolfire, and D. Hollenbach, Astrophys. J. **722**, 1460 (2010).

[33] C. Evoli, D. Gaggero, A. Vittino, G. Di Bernardo, M. Di Mauro, A. Ligorini, P. Ullio, and D. Grasso, JCAP **1702**, 015 (2017), arXiv:1607.07886 [astro-ph.HE].

[34] E. C. Stone, A. C. Cummings, F. B. McDonald, B. C. Heikkila, N. Lal, and W. R. Webber, Science **341**, 150 (2013), http://science.sciencemag.org/content/341/6142/150.full.pdf.

[35] A. C. Cummings, E. C. Stone, B. C. Heikkila, N. Lal, W. R. Webber, G. Jóhannesson, I. V. Moskalenko, E. Orlando, and T. A. Porter, The Astrophysical Journal **831**, 18 (2016).

[36] O. Adriani, , *et al.* (PAMELA), Astrophys. J. **791**, 93 (2014), arXiv:1407.1657 [astro-ph.HE].

[37] M. Aguilar *et al.* (AMS), Phys. Rev. Lett. **117**, 231102 (2016).

[38] D. Gaggero, L. Maccione, D. Grasso, G. Di Bernardo, and C. Evoli, Phys. Rev. **D89**, 083007 (2014), arXiv:1311.5575 [astro-ph.HE].

[39] L. J. Gleeson and W. I. Axford, Astrophys. J. **154**, 1011 (1968).

[40] J. F. Navarro, C. S. Frenk, and S. D. M. White, Astrophys. J. **462**, 563 (1996), astro-ph/9508025.

[41] P. Salucci, F. Nesti, G. Gentile, and C. F. Martins, Astron. Astrophys. **523**, A83 (2010), arXiv:1003.3101 [astro-ph.GA].

[42] P. Ciafaloni, D. Comelli, A. Riotto, F. Sala, A. Strumia, and A. Urbano, Journal of Cosmology and Astroparticle Physics **2011**, 019 (2011).

[43] M. Ackermann *et al.* (Fermi-LAT), Phys. Rev. **D93**, 082001 (2016), arXiv:1604.03349 [astro-ph.HE].

[44] M. Ackermann *et al.* (Fermi-LAT), Phys. Rev. **D91**, 122002 (2015), arXiv:1506.00013 [astro-ph.HE].

[45] R. Brun and F. Rademakers, *New computing techniques in physics research V. Proceedings, 5th International Workshop, AIHENP '96, Lausanne, Switzerland, September 2-6, 1996*, Nucl. Instrum. Meth. **A389**, 81 (1997).

[46] https://root.cern.ch/ release 5.34.

[47] G. Steigman, B. Dasgupta, and J. F. Beacom, Phys. Rev. **D86**, 023506 (2012), arXiv:1204.3622 [hep-ph].

[48] M. Ackermann *et al.* (Fermi-LAT), Phys. Rev. Lett. **115**, 231301 (2015), arXiv:1503.02641 [astro-ph.HE].

[49] M. Ackermann *et al.* (Fermi-LAT), Astrophys. J. **812**, 159 (2015), arXiv:1510.00004 [astro-ph.HE].

[50] H. Abdallah *et al.* (H.E.S.S.), Phys. Rev. Lett. **117**, 111301 (2016), arXiv:1607.08142 [astro-ph.HE].

[51] M. Aguilar *et al.* (AMS), Phys. Rev. Lett. **110**, 141102 (2013).

[52] M. Aguilar *et al.* (AMS), Phys. Rev. Lett. **113**, 121102 (2014).

[53] M. Ackermann *et al.* (Fermi-LAT), Phys. Rev. **D89**, 042001 (2014), arXiv:1310.0828 [astro-ph.HE].

[54] C.-H. Chen, C.-W. Chiang, and T. Nomura, Phys. Rev. **D97**, 061302 (2018), arXiv:1712.00793 [hep-ph].

[55] J. Cao, L. Feng, X. Guo, L. Shang, F. Wang, P. Wu, and L. Zu, Eur. Phys. J. **C78**, 198 (2018), arXiv:1712.01244 [hep-ph].

[56] A. Fowlie, Phys. Lett. **B780**, 181 (2018), arXiv:1712.05089 [hep-ph].

[57] P. Athron, C. Balazs, A. Fowlie, and Y. Zhang, JHEP **02**, 121 (2018), arXiv:1711.11376 [hep-ph].